# Full Time-Domain DORT for Ultrawideband Electromagnetic Fields in Dispersive, Random Inhomogeneous Media

Mehmet E. Yavuz, *Student Member, IEEE*, and Fernando L. Teixeira, *Senior Member, IEEE*

***Abstract*—We investigate the decomposition of the time-reversal operator (DORT under its French language acronym) method applied to ultrawideband electromagnetic pulses propagating in dispersive and (continuous) inhomogeneous random media where volumetric scattering effects are important. We analyze the effects of random medium statistics on the time-reversal operator (TRO) eigenvalues and eigenvectors, and on subsequent selective focusing performance. We develop and employ a full time-domain DORT by tracking the excitation eigenvectors from a singular value decomposition of the TRO over the entire bandwidth of operation. We also study effects of frequency dispersion and conduction losses on the TRO and consider dispersion/loss compensation techniques to improve DORT operation in those cases.**

***Index Terms*—Decomposition of the time-reversal operator (DORT) method, electromagnetic (EM) propagation in random media, selective focusing, time-reversal (TR).**

## I. Introduction

THE invariance of the wave equation under time-reversal (TR) (in lossless and stationary media) can be exploited for detection and localization of scatterers. Techniques exploiting TR invariance were first developed in acoustics [1], and later applied to lithotripsy [2], inverse scattering [3], underwater communications [4], wireless communications [5], [6], electromagnetic (EM) sensing [7], [8] and imaging [9]–[12].

In order to optimize TR techniques, the analysis of the time-reversal operator (TRO) is fundamental. The eigenvalue and corresponding eigenvector structure of the TRO provides information about the scattering scenario under study. The TRO is obtained using the multistatic data matrix (MDM) of a time-reversal array (TRA). In particular, the TRO for isolated spherical EM scatterers has been derived by considering TRAs with dipole antenna elements in [13] and extended targets have been considered in [14]. By performing an eigenvalue decomposition (EVD) of the TRO and using the TRA to transmit signals produced by particular eigenvectors, *selective focusing* of point-like scatterers becomes possible. This strategy forms the basis of the decomposition of the time-reversal operator (DORT under its French language acronym) method [15], [16]. DORT was first applied for EM waves in [17] using time-harmonic waves and full aspect sensor configurations. Analysis of limited aspect configurations (linear arrays) [18], crosswell boreholes [19], and ultrawideband (UWB) operation [20] have further demonstrated the potential of DORT for EM remote sensing.

Most prior work on DORT have assumed homogeneous background media and time-harmonic fields. Robustness of DORT to noise was demonstrated by considering either random phase shifts on scattered fields [17] or by using discrete random media composed of many point-like scatterers [20] only. Effects of background clutter from *continuous* (inhomogeneous) random media (where volumetric scattering effects are important) on *standard TR* have been examined for EM waves in [7]. However, effects of clutter on DORT performance for UWB signals have not been considered yet. Under such conditions, clutter can contaminate both the signal and noise TRO subspaces, which may mask the number of scatterers and hamper selective focusing in DORT.

In practice, many EM remote sensing scenarios involve lossy and frequency dispersive background media, where TR invariance is broken. In those cases, compensation techniques become necessary for TR (and DORT operation). Uniform amplitude compensation over the entire bandwidth has been considered for acoustic signals in the past [21], [22]. An approximate compensation for losses in DORT has also been considered in [19]. More recently, a short-time Fourier transform (STFT) based method has been introduced in [23] to compensate for *frequency-dependent* attenuation due to a homogeneous dispersive background media. Another recent proposal compensates for conductive losses via a numerical TR algorithm [8].

This work has two main objectives. The first is to address the use of *full time-domain* (instead of central-frequency based) DORT in continuous random media and the effects of first- and second-order random medium statistics on the eigenvalue/eigenvector distribution and subsequent selective focusing performance. The second main objective is to study the effects of dispersion and losses on the DORT performance, and extend the compensation technique of [23] for DORT operation in dispersive and *(random) inhomogeneous* media with conductive losses.

For concreteness, we consider UWB EM pulses launched by linear arrays (limited aspect configuration), in a configuration typical of subsurface sensing. Random medium models are based on inhomogeneous soil models having spatially fluctuating random permittivities and Gaussian correlation functions with dielectric permittivity parameters corresponding to clay type soils. Well-resolved, impenetrable scatterers are considered as primary targets. The TRO is explicitly obtained via two- or three-dimensional (2-D or 3-D) time-domain forward simulations.

Manuscript received July 28, 2005; revised April 5, 2006. This work was supported in part by the National Science Foundation (NSF) under Grant ECS-0347502 and in part by the Ohio Supercomputer Center (OSC) under Grants PAS-0061 and PAS-0110.

The authors are with the ElectroScience Laboratory and Department of Electrical and Computer Engineering, The Ohio State University, Columbus, OH 43212 USA (e-mail: yavuz.5@osu.edu; teixeira@ece.osu.edu).

Digital Object Identifier 10.1109/TAP.2006.879196

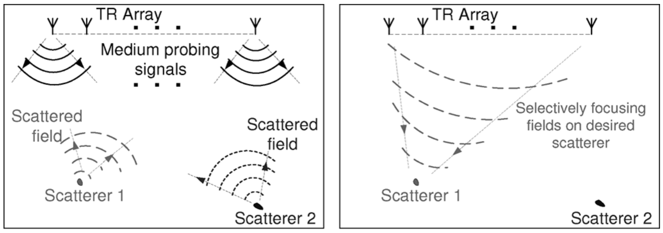


Fig. 1. DORT operation: MDMs are first obtained by launching a short pulse from each TRA antenna and recording the scattered field signals at all the antennas. Selective focusing is achieved by (back-)propagation of the associated eigenvectors from the TRA. (a) Forward propagation for probing the media to obtain MDM, (b) selective focusing via backpropagation of a specific eigenvector.

## II. Full Time-Domain DORT

In media containing multiple discrete scatterers, backpropagation of TR scattered fields results in generation of focal spots on all scatterers simultaneously, and more strongly on the dominant scatterer (*standard TR*). As the standard TR process is iterated, the wavefront becomes increasingly localized on the dominant scatterer [24]. Hence, standard TR iteration does not allow focusing on other (weaker) scatterers unless time-gating is applied. However, time-gating can distinguish only temporally well-resolved scatterers and its performance strongly depends on the usable bandwidth. DORT overcomes this problem by isolating and classifying different scattering centers (in the presence of others) without the need for any time gating or iterative process [15] (Fig. 1). In DORT, a TRA with $N$ transceivers produces an $N \times N$ symmetric (due to reciprocity) MDM denoted as $\boldsymbol{K}(\omega)$ where $\omega$ is the frequency. Since TR operation is equivalent to a phase conjugation in the frequency domain, it can be represented by the Hermitian conjugate $\boldsymbol{K}^\dagger(\omega)$. The TRO is defined as the self-adjoint matrix $\boldsymbol{T}(\omega) = \boldsymbol{K}^\dagger(\omega)\boldsymbol{K}(\omega)$. The singular value decomposition (SVD) of the MDM is given by $\boldsymbol{K}(\omega) = \boldsymbol{U}(\omega)\boldsymbol{\Lambda}(\omega)\boldsymbol{V}^\dagger(\omega)$, where $\boldsymbol{\Lambda}(\omega)$ is the real diagonal matrix of singular values, with $\boldsymbol{U}(\omega)$ and $\boldsymbol{V}(\omega)$ being unitary matrices. Similarly, EVD of the TRO yields $\boldsymbol{T}(\omega) = \boldsymbol{V}(\omega)\boldsymbol{S}(\omega)\boldsymbol{V}^\dagger(\omega)$, where $\boldsymbol{S}(\omega) = \boldsymbol{\Lambda}^\dagger(\omega)\boldsymbol{\Lambda}(\omega)$ is the diagonal matrix of eigenvalues. The eigenvalues of the TRO are equal to the squared singular values of the MDM, and, hence, both terms are used interchangeably in this work.

Columns of the unitary matrix $\boldsymbol{V}(\omega)$ correspond to normalized eigenvectors of the TRO. For well-resolved, point-like acoustic scatterers in homogeneous media, each significant eigenvalue of the TRO is associated to a single scatterer (isotropic scattered fields). Subsequent backpropagation of the corresponding eigenvector yields wavefront focusing on that scatterer [16], as illustrated in Fig. 1. In the EM case, no scatterer produces isotropic EM waves in 3-D and hence multiple eigenvalues can be associated to a single scatterer [13], [17], [18]. In prior works, EVD of the TRO was carried out only by considering the central frequency of operation ($\omega_c$). This approach is denoted here as *central-frequency (CF)-DORT*. In this case, backpropagated fields radiated from the TRA for focusing on the $p$th scatterer are produced by the associated eigenvector $\mathbf{v}_p(\omega_c)$ and singular value $\lambda_p(\omega_c)$ which satisfy $\boldsymbol{T}(\omega_c)\mathbf{v}_p(\omega_c) = \lambda_p^2(\omega_c)\mathbf{v}_p(\omega_c)$. The normalized vector $\mathbf{v}_p(\omega_c)$ is the $p$th column of $\boldsymbol{V}(\omega_c)$. The components of the $N \times 1$ column vector $\mathbf{r}_p(\omega_c)$ give the excitation amplitudes for the $N$ element TRA via $\mathbf{r}_p(\omega_c) = \lambda_p^{-1}(\omega_c)\boldsymbol{K}^\dagger(\omega_c)\mathbf{v}_p(\omega_c)$. In CF-DORT, the same amplitude distribution $\mathbf{r}_p(\omega_c)$ is used along the entire bandwidth. However, for UWB signals a similar decomposition should be applied at each frequency of the entire bandwidth to yield an amplitude distribution (excitation) that is truly frequency dependent. This is particularly important to improve the focusing resolution (super-resolution) of the TR UWB signals by taking advantage of frequency decorrelation due to multiple scattering [17], [25].

When different eigenvalues are associated with the same well-resolved scatterers throughout the entire bandwidth, the corresponding (frequency dependent) eigenvectors can be used to obtain a set of UWB pulses to excite each array element, by means of an inverse Fourier transformation. In particular, the UWB pulses to be fed to the array elements for selective focusing of the (well resolved) $p$th scatterer are given by $\mathbf{r}_p(t) = \mathcal{F}^{-1}(\lambda_p^{-1}(\omega)\boldsymbol{K}^\dagger(\omega)\mathbf{v}_p(\omega))$, where $\mathcal{F}^{-1}$ stands for inverse Fourier transform. This characterizes the full *time-domain (TD)-DORT* employed here. In scenarios with multiple scatterers of similar strength, tracking of the eigenvalue(s) and eigenvector(s) of each scatterer over the entire bandwidth can be done by analyzing the eigenvector(s) behavior, e.g., from the orthogonality between all significant eigenvectors at *adjacent* frequency samples.

## III. Problem Scenario

Initially, we employ 3-D finite-difference time-domain (FDTD) [26] simulations to produce synthetic data from scattering by 3-D objects in random media [27] where TR invariance holds, i.e., both nondispersive and lossless (NDL) media are used. Once the effects of random medium on the TRO structure are studied, 2-D simulations [28] are employed to get the scattering data in both dispersive and conductive (DPC) media to analyze DORT performance under such conditions. FDTD grids with $N_x \times N_y \times N_z = 220 \times 200 \times 250$ and $N_x \times N_y = 360 \times 360$ cells are used for 3-D and 2-D cases, respectively. The FDTD domains are terminated by perfectly matched layers (PML) [29] extended to random media [27] to provide reflectionless truncation of the computational domains.

For 3-D simulations, the random medium has spatially fluctuating permittivity $\epsilon(\bar{r}) = \epsilon_m + \epsilon_f(\bar{r})$. Here, $\bar{r} = x\hat{x} + y\hat{y} + z\hat{z}$ denotes spatial position, and $\epsilon_m$ is the average relative permittivity and equal to 5.5 (dry soil). The fluctuating permittivity $\epsilon_f(\bar{r})$ is a zero mean Gaussian random variable which has a Gaussian correlation function $C(\bar{r_1} - \bar{r_2})$ with variance $\delta$ and transverse (horizontal) and longitudinal (vertical) correlation lengths denoted as $l_s$ and $l_z$, respectively. The Gaussian correlation function is given by

$$\begin{aligned} C(\bar{r}_1 - \bar{r}_2) &= \left\langle \epsilon_f(\bar{r}_1)\epsilon_f^*(\bar{r}_2) \right\rangle \\ &= \delta \exp\left( -\frac{|x_1 - x_2|^2 + |y_1 - y_2|^2}{l_s^2} - \frac{|z_1 - z_2|^2}{l_z^2} \right). \quad (1) \end{aligned}$$

The linear TRA consists of $N = 7$ dipole transceivers. Each dipole is initially fed by current source $\bar{J}_i(x, y, x, t) = \hat{e}_i r_i(t)$

where $\hat{e}_i$ ($\hat{x}$, $\hat{y}$ or $\hat{z}$) is the unit vector representing the polarization of the $i$th dipole and $r_i(t)$ is the UWB time-domain excitation taken as a Blackmann-Harris (BH) pulse derivative [30] centered at $f_c = 400$ MHz. Since the incident electric field on the scatterers is related to the derivative of the current by $\bar{E}^{inc}(\bar{r}, t) = \mu_0 \overline{\overline{G}} * (\partial \bar{J}_i / \partial t)$ where $\overline{\overline{G}}$ is the Green's function and $*$ is convolution in time, the incident field appears as the second derivative of the BH pulse and the central frequency is shifted approximately to 500 MHz. A uniform discretization cell size of $\Delta_x = \Delta_y = \Delta_z (= \Delta_s) = 0.7995$ cm is chosen for the FDTD grid. This corresponds to $\lambda/93$ in free space and $\lambda/40$ for the mean permittivity of the random media at the central frequency (physical dimensions of the grid are $1.75 \times 1.59 \times 1.99$ m$^3$). The TRA lies parallel to the $x$-direction and the dipoles are distributed evenly along an aperture length of $a_{3D} = 120\Delta_s$, with the first dipole at $(x_{t_1}, y_{t_1}, z_{t_1}) = (50, 100, 40)\Delta_s$. To isolate volumetric scattering effects, surface roughness and mutual interactions among array elements are not included. We should point out that the results presented depend on the size of the computational box used for the random medium, which is essentially limited by the computational resources at our disposal. These truncation effect decrease for larger computational boxes or smaller permittivity variances. In the setup considered, this dependency is weak because the boundary reflections affect the received signals at very later times and with relatively very small amplitudes.

As for the 2-D simulations, only $TM_z$ case is considered to guarantee isotropic scattering from point-like scatterers. Frequency dispersion is modeled by an $M_s$-species inhomogeneous Lorentz model for the complex permittivity function:

$$\epsilon(\bar{r}, \omega) = \epsilon_0 \epsilon_\infty(\bar{r}) + \epsilon_0 \chi(\bar{r}, \omega) - \sigma / j\omega \qquad (2)$$

with

$$\chi(\bar{r}, \omega) = \sum_{p=1}^{M_s} G_p \omega_p^2 \frac{\epsilon_s(\bar{r}) - \epsilon_\infty(\bar{r})}{\omega_p^2 - i2\omega\alpha_p - \omega^2} \qquad (3)$$

where $\chi(\bar{r}, \omega)$ is the medium susceptibility, $\omega_p (= 2\pi f_p)$ is the resonant frequency for the $p$ species, $\alpha_p$ is the corresponding damping factor, $G_p$'s are constants satisfying $\Sigma_{p=1}^{M_s} G_p = 1$, $\sigma$ is the static conductivity, $\epsilon_s(\bar{r})$, $\epsilon_\infty(\bar{r})$ are the static and infinite frequency permittivities, respectively and $z = 0$, i.e., $\bar{r} = x\hat{x} + y\hat{y}$. Note that $\epsilon_\infty(\bar{r})$ is a misnomer, and simply represents the limit of $\epsilon(\bar{r}, \omega)$ for larger $\omega$ in the *finite* range of frequencies considered by the model. In the above, $\epsilon_\infty(\bar{r}) = \epsilon_m + \epsilon_f(\bar{r})$ where $\epsilon_m$ is the average relative infinite frequency permittivity, $\epsilon_f(\bar{r})$ is a zero mean Gaussian random variable, and $\epsilon_s(\bar{r})$ has the same distribution as $\epsilon_\infty(\bar{r})$ except having a different mean $\langle \epsilon_s(\bar{r}) \rangle = \epsilon_m + \Delta_\epsilon$ where $\Delta_\epsilon > 0$ to guarantee that the medium is passive.

A linear TRA lying parallel to the $x$-direction is used with $N = 11$ $z$-directed dipole transceivers. A uniform spatial cell size of $\Delta_s = 1.0$ cm is used in the FDTD grid, yielding a $3.6 \times 3.6$ m$^2$ physical domain overall size. The dipoles are evenly distributed along an aperture length of $a_{2D} = 160\Delta_s$ with the first one positioned at $(x_{t_1}, y_{t_1}) = (100, 35)\Delta_s$. The realistic soil parameters given in Table I are used for the Lorentz model. These parameters are obtained by curve fitting a two-species Lorentz model to the experimental data reported in [31] and a Debye model as reported in [28] for Puerto Rico type of clay loams. The damping factors are $\alpha_1 = \sqrt{2}\omega_1$, $\alpha_2 = \sqrt{2}\omega_2$ and $G_1 = 0.75$, $G_2 = 0.25$. Note that by an appropriate choice of parameters, the Lorentz model reduces to the Debye model. Since the former model is more general, it is the one employed here [28]. The same setup is also used for the simulation of the nondispersive ($\chi(\bar{r}, \omega) = 0$) and lossless ($\sigma = 0$) case to provide a reference solution where the permittivity ($\epsilon_r(\bar{r})$) is real and chosen as $\epsilon_r(\bar{r}) = \epsilon_\infty(\bar{r})$.

TABLE I
LORENTZ-MODEL PARAMETERS OF THE PUERTO RICO TYPE CLAY LOAMS. (UP TO 1 GHz RANGE)

| Moisture | $\langle \epsilon_s(\bar{r}) \rangle$ | $\langle \epsilon_\infty(\bar{r}) \rangle$ | $\sigma (mS/m)$ | $f_1$ (MHz) | $f_2$ (MHz) |
|---|---|---|---|---|---|
| 2.5% | 4.25 | 3.54 | 0.397 | 130.39 | 330.58 |
| 5.0% | 6.55 | 4.76 | 1.110 | 95.39 | 336.58 |
| 10.0% | 9.50 | 6.67 | 2.000 | 90.39 | 416.58 |

Kramers-Kronig relations [32] imply that any permittivity function with frequency variations exhibits a non-zero imaginary part (attenuation). Any additional phase shift produced by frequency dispersion and/or losses is exactly compensated during TR (a phase conjugation in the frequency domain), but amplitude attenuation affects the TR signals during both forward and back-propagations. This attenuation degrades the focused signals relative to the nondispersive (lossless) case. This can be partially overcome by a compensation technique that acts as an inverse filter with respect to the attenuation. Such a technique has been proposed in [23] and utilizes *time-dependent* windowed filters based on STFT. If the medium is homogeneous, these filters can be easily obtained. However, for random media with inhomogeneous dispersive and conductive characteristics, approximate filters should be employed instead.

For both set of simulations, random medium realizations are produced using the approach described in [27]. Because of statistical stability of the TRO [33], a single realization is used for each result. Throughout this work, the number of well-resolved point-like scatterers ($M$) is assumed to be less than the number of antennas of the TRA, i.e., $N > M$. This would imply in a TRO matrix of rank $M$ for isotropic scattering (i.e., in the acoustic case or 2-D $TM_z$ case), but the rank may be larger than $M$ in the 3-D EM case [13].

## IV. DORT IN RANDOM MEDIA

Among the attractive properties of a TRA is that multiple scattering in the intervening medium *increases* the effective aperture [25], [34], or equivalently, the refocusing resolution. Here, we consider similar effects due to both full polarimetric operation and random medium statistics on the (full) TD-DORT. We initially consider the effects of both first- and second- order statistics on singular value (eigenvalue) distribution of the MDM (TRO) obtained in 3-D NDL random media.

### A. Discrete Scatterer in NDL Homogeneous Media

For reference, we first analyze the TRO of a single spherical PEC scatterer with radius $r = 4.79$ cm centered at

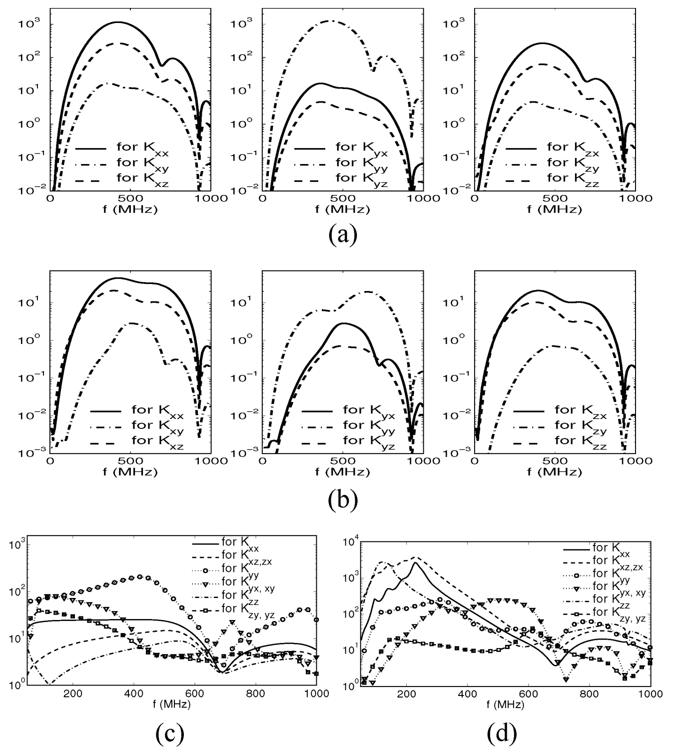


Fig. 2. Significant singular values (and their ratios) of the MDMs $\boldsymbol{K}_{ij}$ in a NDL *homogeneous* medium. A single spherical PEC scatterer is considered. For this particular configuration, $\boldsymbol{K}_{yy}$ allows the most isotropic scattering. (a) First singular values ($\lambda_{ij_1}$), (b) second singular values ($\lambda_{ij_2}$), (c) ratio of first and second singular values ($\lambda_{ij_1}/\lambda_{ij_2}$), (d) ratio of second and third singular values ($\lambda_{ij_2}/\lambda_{ij_3}$).

$(x_{s_1}, y_{s_1}, z_{s_1}) = (110, 100, 200)\Delta_s$ in an homogeneous medium. Linear TRAs are employed under three orthogonal linear polarizations. Both scatterer and the TRA lie on the same $y$-plane. For each $j$-polarized incident field ($j = x, y, z$), three scattered field components are produced. Therefore, the full polarimetric TRA response consists of a total of nine MDMs, $\boldsymbol{K}_{ij}$, $i, j = x, y, z$. However, by reciprocity only six of them are independent as observed in Fig. 2 where the first two significant singular values of all MDMs are plotted over frequency. The remaining ones are not shown here since they are insignificant compared to the first two. It is observed that, for this TRA and scatterer configuration, $\boldsymbol{K}_{yy}$ allows for a more isotropic scattering compared with other polarization combinations. This case is similar to the acoustic or a 2-D EM case with perpendicular polarization ($TM_z$ or s-polarization) [18]. This can also be noticed from the ratios between the first and second significant eigenvalues as shown in Fig. 2(c), with the maximum ratio obtained for $\boldsymbol{K}_{yy}$. Therefore, we can conclude that only one significant singular value is present for $\boldsymbol{K}_{yy}$, but two significant singular values are observed for $\boldsymbol{K}_{xx}$, $\boldsymbol{K}_{xz}$, $\boldsymbol{K}_{zx}$ and $\boldsymbol{K}_{zz}$. Having more than one significant singular value for a single scatterer is simply a consequence of non-isotropic scattering for a particular polarization combination [13], [17]. The remaining TRA polarization combinations do not provide comparably significant data due to weak scattered signals. This can also be concluded by observing the ratio between the second and third singular values in this configuration, as shown in Fig. 2(d), which is considerably larger than that between the first and second ones over the entire frequency band.

### B. Discrete Scatterer in NDL Random Media

Next, a single spherical PEC scatterer is considered in Gaussian random media having different first- and second-order statistics.

*1) Effect of First-Order Statistics:* The effect of random medium variance on the singular values is first investigated. MDMs corresponding to different polarized TRAs are obtained in random media with fixed correlation lengths ($l_s = l_z = 8\Delta_s = 6.33$ cm) and variance ($\delta$) changing between 0.1, 0.5 and 1.0 which represent approximately 30%, 54%, and 81% of $\epsilon_m (= 5.5)$, respectively. The first three singular values for $\boldsymbol{K}_{xx}$, $\boldsymbol{K}_{yy}$, $\boldsymbol{K}_{zz}$ and $\boldsymbol{K}_{zx}$ are plotted in Fig. 3. As it can be observed, for larger variances, the magnitudes of the singular values increase. Moreover, other significant singular values may also appear. These can often be distinguished as clutter as long as they are much smaller than the significant ones corresponding to (primary) discrete scatterers. Once the time-domain signals produced using TD-DORT applied to $\boldsymbol{T}_{yy} = \boldsymbol{K}_{yy}^{\dagger}\boldsymbol{K}_{yy}$ are transmitted from the TRA, the resulting wave fields converge and interfere constructively around the intended scatterer location. We show snapshots of $E_y$ at the focal time for homogeneous and random media cases in Fig. 4, where the grayscale mapping described in [35] is used. In addition, a cross-range field pattern defined by

$$D_{E_y}(x) = \frac{1}{N_2 - N_1} \sum_{i=N_1}^{N_2} E_y^2(x, y_s = 100\Delta_s, z = i\Delta_s) \quad (4)$$

is shown for homogeneous and random media for various variances and fixed correlation length. Here, $N_1 = 160$ and $N_2 = 220$, so that whole focusing spot is included.

For the range of variances considered, the field produces a larger peak in the focal spot for increasing variances, as shown in Fig. 4. This can be attributed to an increase in the *frequency decorrelation* among the different frequency components of the UWB field due to multiple scattering and to the *phase conjugation* enforced by TR. This produces a *coherent* summation (over the entire bandwidth) of different frequency components of the field only nearby the focal point, and an *incoherent* summation elsewhere [7], [25], [34]. Moreover, when they are compared in a normalized fashion, the focal spot becomes slightly narrower for larger variances, as also shown in Fig. 4. This latter phenomena is caused by *spatial decorrelation* due to increasing multiple scattering. Equivalently, this produces an increase on the effective aperture of the TRA, characterizing superresolution [25]. This directivity gain (over the homogeneous case) for the pattern defined in (4) is equal to 1.21 for $\delta = 1.0$.

*2) Effect of Second-Order Statistics:* Additional simulations are performed to evaluate the effect of different correlation lengths on the singular value distribution and subsequent focusing. Here, the correlation length of the random medium with fixed variance of $\delta = 0.5$ is progressively increased from $l_s = 3.2$ cm ($4\Delta_s$) to $l_s = 11.2$ cm ($14\Delta_s$) where $l_s = l_z$. Significant singular values for different TRA combinations are shown in Fig. 5. Generally speaking, it is observed that larger

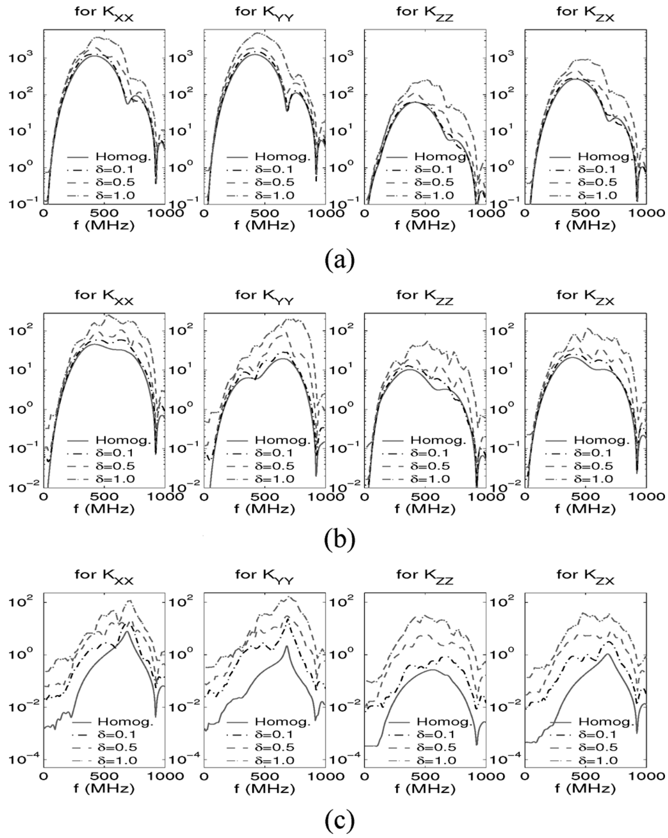


Fig. 3. Three most significant singular values of the MDMs $\boldsymbol{K}_{ij}$. The singular values are obtained in NDL *random media* with increasing variance and fixed correlation lengths. A single PEC scatterer is embedded within the media. (a) First singular values ($\lambda_{ij_1}$), (b) second singular values ($\lambda_{ij_2}$); (c) third singular values ($\lambda_{ij_3}$).

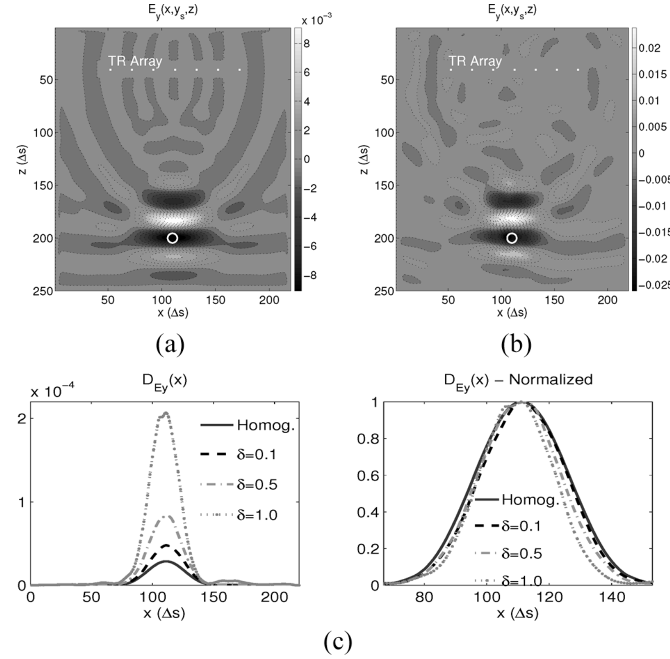


Fig. 4. Spatial distribution of the focused $y$-component of the electric field ($E_y$) at $xz$-plane ($y = 100\Delta_s$) and cross-range patterns $D_{E_y}(x)$ at the time of first minimum focusing. The TRA antennas are fed with the time-domain signals generated by the highest eigenvalue and corresponding eigenvector of the TRO obtained using $\boldsymbol{K}_{yy}$. The scatterer location is denoted by a small circle. (a) Homogeneous medium, (b) random medium ($\delta = 1.0, l_s = l_z = 8.0\Delta_s$), (c) focused $E_y$ at cross-range, and corresponding normalized amplitudes in various random media with increasing variances.

correlation length yield smaller singular values. This can be explained from the fact that media with larger correlation lengths produce less multiple scattering (in this range of correlation lengths).

### *C. Multiple Well-Resolved Scatterers in Random Media*

In this case, two PEC spheres with radii $r_1 = 3.99$ cm and $r_2 = 3.18$ cm are centered at $(x_{s_1}, y_{s_1}, z_{s_1}) = (50, 100, 160)\Delta_s$ (first scatterer) and $(x_{s_2}, y_{s_2}, z_{s_2}) = (150, 100, 180)\Delta_s$ (second scatterer), respectively. This is a well-resolved configuration, i.e., the contribution from multiple scattering *between* the scatterers is much lower than first-order scattered signals. If multiple scattering between the scatterers were not negligible, then the significant eigenvalues would not correspond to individual scatterers but to some linear combination. A possible remedy to reduce multiple scattering between the discrete embedded scatterers in that case would be to form the MDMs *after* applying iterative time-reversal a certain number of times. As mentioned elsewhere [24], iterative TR works as a power SVD method and therefore, the highest eigenvalue dominates as the number of iterations goes to infinity. We also note that some techniques that can naturally incorporate multiple scattering between targets (in the time-harmonic regime) have been presented in [9], [10], [36] and references therein.

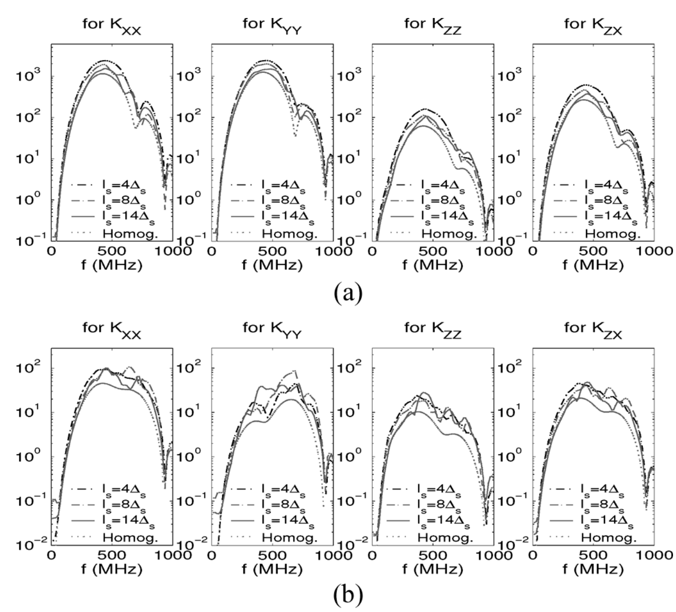


Fig. 5. Significant singular values of $\boldsymbol{K}_{ij}$ obtained in various NDL random media with different correlation lengths ($l_s = l_z$) and fixed variance. A single spherical PEC scatterer is present. (a) First singular values ($\lambda_{ij_1}$), (b) second singular values ($\lambda_{ij_2}$).

The TRO singular values for different TRA polarization combinations are shown in Fig. 6, for both homogeneous and random media. It can be observed that in both media two significant singular values can be distinguished for $\boldsymbol{K}_{yy}$. For the other cases, there are no such clear amplitude separation of

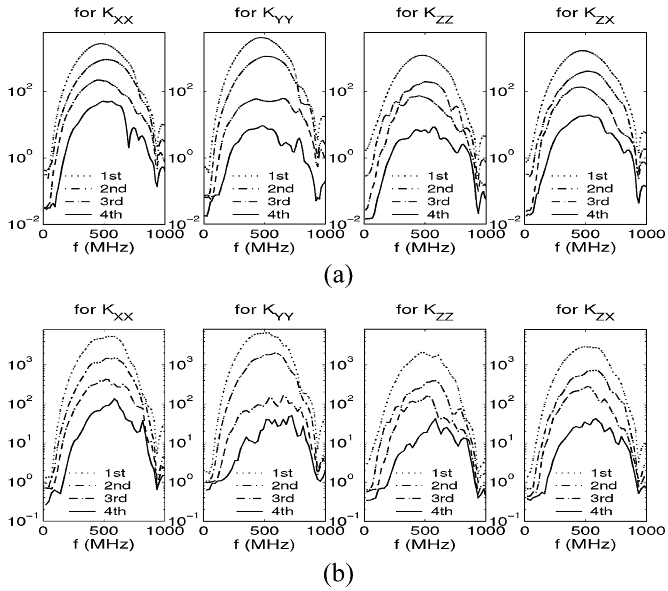


Fig. 6. First four singular values of $\boldsymbol{K}_{ij}(\omega)$ obtained in homogeneous and random media with two embedded spherical PEC scatterers. (a) Homogeneous medium, (b) random media with $\delta = 0.5, l_s = l_z = 8\Delta_s$.

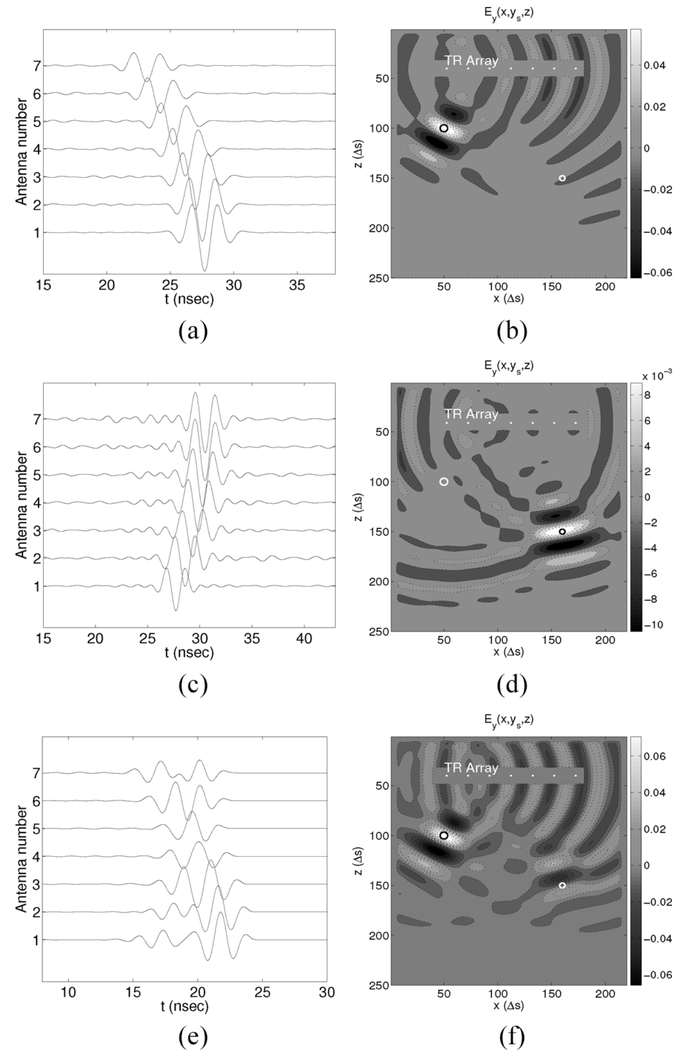


Fig. 7. Left column: time-domain signals used in the backpropagation step from the TRA. Right column: corresponding spatial distribution of the $y$-component of the electric field ($E_y$) at $xz$-plane ($y = 100\Delta_s$) at the time of focusing. Time-domain signals are obtained using $\boldsymbol{K}_{yy}$ for homogeneous medium and shown here normalized to unity. The scatterer locations are indicated by small circles. (a) Time-domain signals from first eigenvalue and eigenvector, (b) focusing on first scatterer, (c) time-domain signals from second eigenvalue and eigenvector, (d) focusing on the second scatterer, (e) time-domain signals from standard TR using the $7^{th}$ antenna element for initial excitation, (f) focusing on both scatterers, i.e., no selective focusing.

the first two singular values with respect to the others, and all four singular values are within a smaller degree of (successive) amplitude separation. Analysis of the phase distributions of the eigenvectors at the whole bandwidth shows that, for the $\boldsymbol{K}_{yy}$ case, the first and second eigenvalues are associated with the first and second scatterer, respectively. On the other hand, two significant singular values exist for each of the individual scatterer in the other cases. Using the first two dominant eigenvalues and corresponding eigenvectors of $\boldsymbol{T}_{yy}$, the time-domain signals to be transmitted by the TRA antennas are shown in left column of Fig. 7. Once these signals are transmitted by the TRA, they propagate and *selectively* focus around the associated original scatterer locations, as shown on the right column of Fig. 7. The standard TR result is also shown on the last row, where the rightmost antenna ($7^{th}$ from left) is used for initial excitation. In this latter case, received signals at the TRA are simply time-reversed and backpropagated without any additional pre-processing. Since the signatures of both scatterers are included in these backpropagated signals, focusing occurs on *both* scatterers (and more strongly on the dominant scatterer). As noted before, standard TR can achieve selective focusing by time-gating. However, this is limited to scenarios where the signatures of each scatterer are resolved in time. Additionally, it should be pointed out that time-gating suppresses some multipath contributions and thus can reduce superresolution. Finally, it is observed that changes on the variance or correlation length produce effects similar to the single scatterer case in Section IV-B, and are not shown here.

## V. DORT in Random, Dispersive Media With Conductive Losses

The previous section assumed NDL media. However, in many realistic situations, intervening media have dispersion and/or conductive losses breaking the TR invariance (e.g., soil, breast tissue, etc.). Although the basic implementation of the DORT method in DPC media is somewhat similar to the NDL case, the effects of dispersion and losses have to be considered in order to adequately interpret the eigenvalues and eigenvectors and later correctly use them in the DORT method. In this section, we study those effects and apply compensation techniques to improve the DORT method performance in dispersive and conductive media. Simulations are carried out in 2-D without loss of generality.

### A. TRO Behavior in DPC and NDL Homogeneous Media

We first compare the TRO obtained for a single cylindrical PEC scatterer with radius $r = 4.0\Delta_s$ centered at $(x_{s_1}, y_{s_1}) = (180, 170)\Delta_s$ for both DPC (for moisture level of 2.5%) and NDL *homogeneous* ($\delta = 0$) media. In both cases, we obtain $\boldsymbol{K}_{zz}$ whose first two singular value distributions are shown in

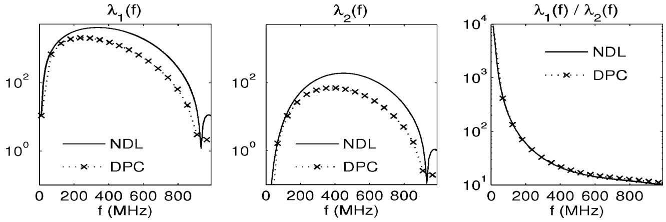


Fig. 8. First and second singular value distributions ($\lambda_1$ and $\lambda_2$) of $\boldsymbol{K}_{zz}$ obtained for a single cylindrical PEC scatterer in DPC and NDL *homogeneous* backgrounds. The ratio $(\lambda_1/\lambda_2)$ is also shown.

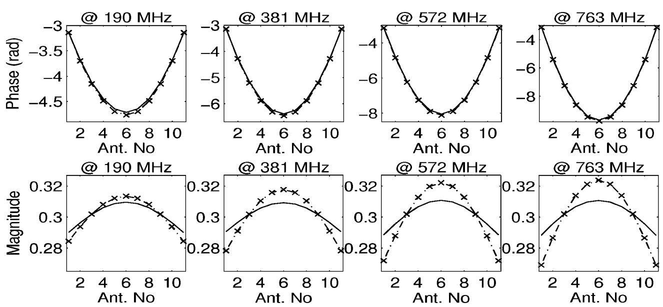


Fig. 9. Phase and magnitude distribution of the first eigenvector for each TRA antenna at several frequencies along the bandwidth. (Solid line: NDL case. Dash-dotted line: DPC case).

Fig. 8 (others are much smaller than these, hence not shown). Dispersion and losses (attenuation) decrease the singular values. As expected, this effect becomes more pronounced at higher frequencies. The ratios of the first and second singular values remain almost the same. This large ratio implies that there is only one significant singular value corresponding to a single scatterer in the medium [16]. Once the eigenvectors at different frequencies along the bandwidth are analyzed, it is observed that despite the decrease on the singular value magnitudes, relative phase distribution among the array elements is preserved. In Fig. 9, phase and magnitude distributions of the first eigenvector versus TRA antennas are shown at several frequencies along the bandwidth (Similar behavior is also observed at other frequencies but not shown here). The scatterer location along the cross-range can be estimated from these distributions [18], [20]. These singular values and eigenvectors are employed in the TD-DORT to generate the signals to be retransmitted from the TRA. The resulting spatial distribution of the $E_z$ field components at the time of focusing are shown in Fig. 10 for both DPC and NDL media. In both cases, selective focusing around the original scatterer is observed. However, focusing performance is degraded in the DPC case, as clear from the cross-range profile (note, in particular, the decrease in cross-range resolution). Therefore, compensation techniques become of interest to improve performance, as presented next.

### *B. Dispersion and Loss Compensation for DORT in Dispersive, Inhomogeneous Media With Conductive Losses*

Effects of the random medium statistics on the TRO were considered for the NDL case in the previous Section. It was verified that factors increasing multiple scattering improve the

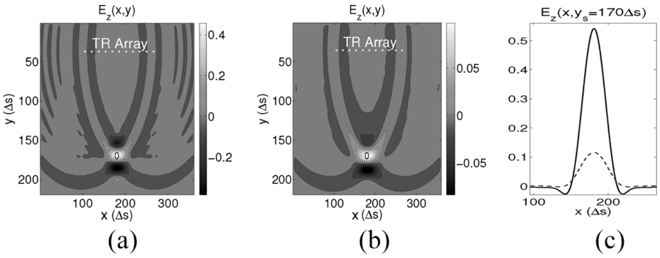


Fig. 10. Spatial distribution of the $E_z$ field component in the $xy$-plane and at cross-range ($y_s = 170\Delta_s$) due to time-domain signals produced by the largest eigenvalue and corresponding eigenvector in both DPC and NDL homogeneous media. (Solid line: NDL case, dash-dotted line: DPC case). The scatterer location is indicated by a small circle. (a) NDL, (b) DPC, (c) cross-range.

focusing resolution (superresolution). Similar behavior is also observed in DPC case but not shown here for the sake of brevity.

In DPC media, UWB signals transmitted from each TRA antenna undergo attenuation. When the background medium is *homogeneous*, this attenuation can be partially compensated using the approach described in [23]. However, in the case of *inhomogeneous* background media (as encountered in practice), the attenuation depends on position in general. Unless the characteristics of the medium are known pointwise (which is not a realistic assumption), it is not possible to find *exact* filters to compensate the losses in this case. The weaker assumption here is that only first- and second- order statistics of the medium are known. In this case, *approximate* compensation filters can be found as described next.

To simulate the attenuation undergone in the original DPC random medium, multiple realizations of the random medium are employed. An UWB signal is transmitted from a point source in the test media and a set of received signals are recorded at increasing distances. We denote the resulting distance-versus-time collection of traces as *DvT plots*. For each realization of the random test media, the total electric field at a specific distance is written as

$$\bar{E}(\bar{r}) = \bar{E}_{inc}(\bar{r}) + \int_v d\bar{r}'\overline{\overline{G}}(\bar{r},\bar{r}')\cdot o(\bar{r}')\bar{E}(\bar{r}') \tag{5}$$

where $\bar{r}$ is the distance between the source and observation points, $\bar{E}_{inc}(\bar{r})$ is the incident field (invariant for all realizations), $\overline{\overline{G}}$ is the Green's function for an *homogeneous* medium (which may include a static conductivity) having relative dielectric permittivity $\epsilon_m$, and $o(\bar{r}) = \omega^2\mu_0(\epsilon(\bar{r})-\epsilon_m)$ is the contrast function, which depends on the random fluctuations (function of each particular realization). An *average* DvT plot can be obtained by taking the (ensemble) average of the DvT plots of the different realizations. On the other hand, the ensemble averaged field can be written as

$$\left\langle\bar{E}(\bar{r})\right\rangle_{N_e} = \bar{E}_{inc}(\bar{r}) + \int_v d\bar{r}'\overline{\overline{G}}(\bar{r},\bar{r}')\cdot\left\langle o(\bar{r}')\bar{E}(\bar{r}')\right\rangle_{N_e} \tag{6}$$

where $\langle\cdot\rangle_{N_e}$ denotes an *ensemble average* over $N_e$ realizations of a random variable, i.e., $\langle\xi\rangle_{N_e} = N_e^{-1}\sum_{i=1}^{N_e}\xi_i$. For weak

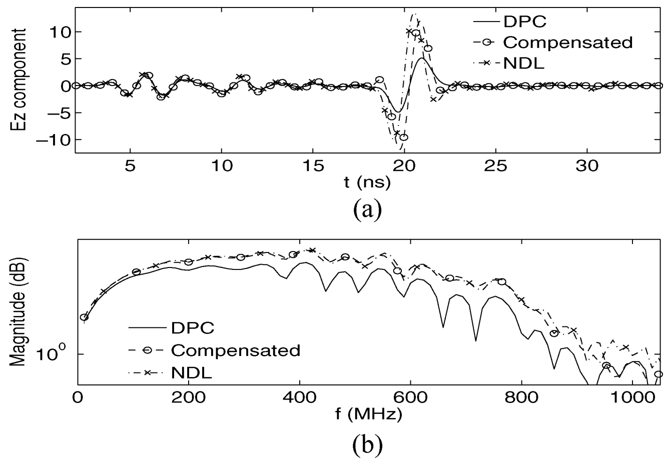


Fig. 11. Comparison of the (*i.*) received signal at one of the TRA antennas ($k_{(1,4)}(t)$) in DPC random medium without compensation), (*ii.*) its compensated version, and (*iii.*) a reference signal that would have been received if the medium were NDL. Both time and frequency domain representations are shown. The random medium has $\delta = 0.026$ and $l_s = 3\Delta s$. The received signals are windowed using Hamming windows of length $256\Delta t$ and overlapping factor of 0.5 [23]. (a) Time-domain, (b) frequency content.

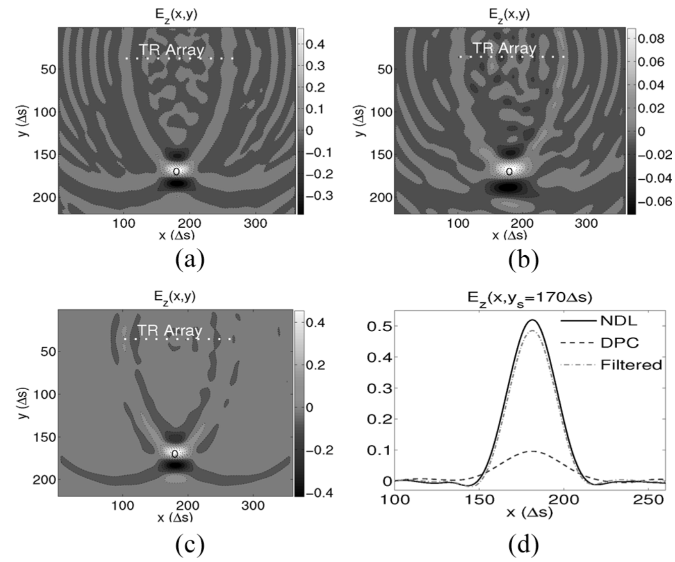


Fig. 12. Spatial distribution of $E_z$ field component in the $xy$-plane and at cross-range ($y_s = 170\Delta_s$) in both DPC (with and without compensation) and NDL random media with $\delta = 0.026$ and $l_s = 3.0\Delta_s$. The scatterer location is indicated by a small circle. (a) NDL, (b) DPC (no compensation), (c) DPC (compensation via filters), (d) cross-range.

fluctuations, we can apply a Born approximation [37] to linearize the dependency of $\langle \bar{E}(\bar{r}) \rangle_{N_e}$ on $\langle o(\bar{r}) \rangle_{N_e}$, and write the ensemble averaged electric field as

$$\left\langle \bar{E}(\bar{r}) \right\rangle_{N_e} \approx \bar{E}_{inc}(\bar{r}) + \int\limits_v d\bar{r}' \overline{\overline{G}}(\bar{r}, \bar{r}') \cdot \langle o(\bar{r}') \rangle_{N_e} \bar{E}_{inc}(\bar{r}'). \tag{7}$$

Under this assumption, the ensemble average of the random media properties can be used to approximate the average electric field response. For a sufficiently large number of realizations, the average response in this approximation approaches that of an homogeneous medium with $\epsilon_{s_{ens}} = \langle \epsilon_s(\bar{r}) \rangle_{N_e}$ and $\epsilon_{\infty_{ens}} = \langle \epsilon_\infty(\bar{r}) \rangle_{N_e}$. Therefore, DvT plot of an homogeneous medium with $\epsilon_{s_{ens}}$ and $\epsilon_{\infty_{ens}}$ can be used to obtain approximate time-dependent filters for weak fluctuations. Note that this Born approximation is assumed only in the process of obtaining *approximate* compensation filters, and not for obtaining the TRO itself or for actual backpropagation.

Associated with DvT plots, compensation filters can be constructed as described in [23] to partially compensate for the losses. This is shown in Fig. 11, where the compensation is applied in one of the TRA received signals. As shown in Fig. 11(a), the received signal from the PEC scatterer is centered at around 20 ns. In the DPC case, the signal amplitude is much weaker than the NDL case. By applying the (time-dependent) compensation, the scatterer signal is considerably amplified. Note that a comparable amplification is not produced on the clutter signal present at earlier and later times.

The compensation filters are zero-phase filters since phase delay is automatically compensated by TR. Note that, for scattering applications, an additional pre-compensation is needed for the backpropagation step [23]. Compensation filters also amplify additive noise within the signal window, and hence cannot not be applied as a remedy in cases where dispersion and losses (attenuation) would reduce the signal-to-noise ratio (SNR) below acceptable levels. Note that only impenetrable scatterers are considered here as primary targets. Because penetrable scatterers have frequency-dependent reflectivity, the present compensation cannot be applied as is.

In Fig. 12, the spatial distributions at the focal time of the $E_z$ field components in DPC and NDL random media ($\delta = 0.026$ and $l_s = 3.0\Delta_s$) are given for the cases with and without compensation. As observed from Fig. 12, the performance can vary for each realization, but compensation yields a better performance than the case without compensation (in terms of closeness to NDL case). A performance study is discussed next.

### C. Compensation Performance

It is important to point out that the approximate compensation filters are not specific to a particular realization, but depend only on the statistics. However, the actual performance of the dispersion compensation depends on several factors, such as the amount of losses (e.g., from the moisture level in the soil), the scatterer location (e.g., depth), and the amount of fluctuations on the complex permittivity (which impacts the validity of Born approximation).

For cases where the propagation distance $d$ is much larger than the correlation length $l_s$, the overall attenuation undergone in random media with different correlation lengths having the same variance approaches to each other. This is due to the fact that for larger distances signals *effectively see* the same attenuation and this attenuation converges to that observed in a homogeneous medium whose dispersion and conductivity values are equivalent to the corresponding mean values of the considered random media. In other words, for $d/l_s \gg 1$, the attenuation produced by each realization depends only on the first-order statistics of the conductivity distribution. This is illustrated in Fig. 13, where the total energy of a UWB pulse as it propagates in media with *random conductivity* (and constant permittivity) having different $l_{s_\sigma}$ and $\delta_\sigma$ is computed versus the

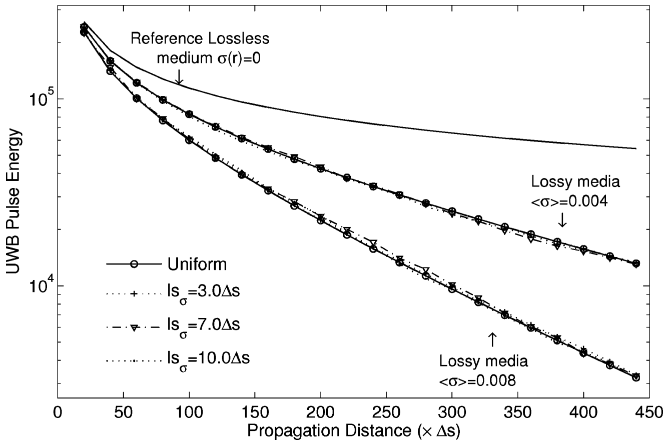


Fig. 13. UWB pulse energy in media with homogeneous permittivity ($\epsilon_r = 5.5$) and random conductivity, for various correlation lengths $l_{s_\sigma}$ and variances $\delta_\sigma$ (a single realization result is plotted). Two different sets of mean/variance are considered (the means are as indicated). The same inset legend is used for both sets of mean/variance values. The lossless ($\sigma(\bar{r}) = 0$) case is also shown as reference.

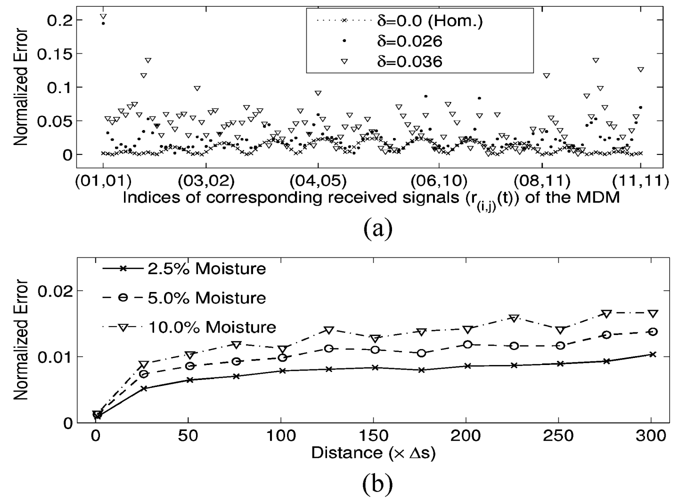


Fig. 14. Normalized error between compensated signals in DPC random media and reference signals in NDL random media for different fluctuations, moisture levels, and scatterer distances. (a) Normalized error for each MDM element signal in random media with fixed embedded scatterer and correlation length $l_s = 3.0\Delta_s$, and various $\delta$ values, as indicated. A Puerto Rico type soil with moisture level 2.5% is employed, (b) normalized error for each MDM element signal in random media for various scatterer distances and moisture levels in a random medium with $l_s = 3.0\Delta_s$ and $\delta = 0.026$.

propagation distance. In this case, $\sigma(\bar{r})$ is a truncated (positive at all points) Gaussian random variable with Gaussian correlation function $C_\sigma(\bar{r}_1 - \bar{r}_2) = \delta_\sigma \exp(-|(\bar{r}_1 - \bar{r}_2)/l_{s_\sigma}|^2)$. Hence, it has a nonzero mean conductivity ($\langle\sigma\rangle$) varying with $\delta_\sigma$. Note that random conductivity characteristic of this homogeneous medium (i.e. constant $\epsilon$) can be considered as a simple model for the random attenuation undergone in an inhomogeneous medium (i.e., random $\epsilon(\bar{r})$) with dispersion and conductivity. For reference, the decay rate in the lossless case ($\sigma(\bar{r}) = 0$) and uniform lossy ($\sigma(\bar{r}) = \langle\sigma\rangle$) cases are also shown in the figure. As observed, the decay rate with respect to the mean conductivity (or $\delta_\sigma$) is much more pronounced than that with respect to different $l_{s_\sigma}$ (for fixed $\delta_\sigma$). Actually, this dominant attenuation is the factor considered during the design process of the compensation filters. Therefore, these results suggest that although negligible local variations may exist, compensation filter performance in randomly conductive media approaches that of the homogeneous case with uniform conductivity for propagation distances sufficiently larger than the correlation length.

However, the use of compensation filters in this case poses additional challenge in terms of the validity of the Born approximation (in addition to the overall degree of attenuation). For Born approximation to hold, the second term of right hand side of (6) should be much smaller than the first term. Since UWB signals are used, the higher frequency components should be considered vis-a-vis the condition $k_H L \langle\Delta_\epsilon\rangle_{N_e}/\epsilon_m \ll 1$ for $k_H L \gg 1$ [37], where $L$ is the maximum propagation distance considered and $k_H = \omega_H^2 \epsilon_m \mu_0$ is the largest wavenumber of interest. This imposes a stringent condition on the level of fluctuations amenable for compensation if a single realization is used to obtain the filters. Thanks to the ensemble averages, $\langle\Delta_{\epsilon,\sigma}\rangle_{N_e} \to 0$ for $N_e \to \infty$, rendering the Born approximation still adequate for *obtaining the filters*. However, the filter performance will degrade for increasing fluctuation levels (i.e., increased variance $\delta$, having other parameters fixed). This is shown in Fig. 14(a) where the normalized error distribution of each MDM element is plotted for homogeneous and random media with increasing variance. This error measure is defined here as $e_I = (\int |s_{ref}(\omega) - s_{cmp}(\omega)| d\omega) / \int |s_{ref}(\omega)| d\omega$, where $s_{ref}$ represents the signal received in the reference NDL media and $s_{cmp}$ is the compensated one in DPC media. Since the random media used differ only in the variance values and share the same ensemble averaged medium, the same set of filters is used for compensation. As the fluctuations increase, the filters become relatively less effective.

Note that, since additive noise present in the system is amplified by the compensation filters, the error between compensated signals and reference signals is naturally expected to increase with increasing signal attenuation. This is illustrated in Fig. 14(b) where $e_I$ at different distances and moisture levels (both affecting the overall signal attenuation) is plotted for a random media with $\delta = 0.026$ and $l_s = 3\Delta_s$.

An alternative approach that compensates for medium losses uses synthetic data from numerical simulations where the sign of the conductivity term is reversed (active-like medium) [8]. This requires pointwise knowledge of the medium conductivity at all spatial points, and can be extended to the Lorentz or Debye dispersive media considered here by reversing the sign of the damping factors, e.g., $\alpha_p$. As long as the original attenuation is small and required backpropagation distance is not large, this approach can compensate for the dispersive and conductive effects. This compensation technique is limited to small losses because the resulting initial-value problem becomes ill-posed.

## VI. Summary and Conclusion

We have discussed the application of full time-domain DORT for UWB electromagnetic waves in 3-D continuous random media. Linear dipole antenna arrays with different polarizations are used to obtain limited aspect MDMs and construct the TRO. The number of well-resolved scatterers and their locations can be determined, and selective focusing can be achieved via backpropagation of fields excited by TRO eigenvectors (associated with the significant singular values). In the full time-domain DORT, the time-domain signals are generated from the TRO eigenvectors by employing the full bandwidth available, instead of only central frequency data.

The effects of first- and second-order (Gaussian) random medium statistics on TRO eigenvalues and corresponding eigenvectors were considered. It has been found that multiple scattering effects in the intervening continuous random media increases the effective aperture of the TRA through spatial decorrelation. For the range of parameters considered, increase in multiple scattering can result from an increase on the variance of the background permittivity or from a decrease on the correlation length. Increase in multiple scattering also allows for enhanced frequency decorrelation among the different frequencies of the UWB probing signal. This produces enhanced focusing on the target location because of phase conjugation enforced by TR. At the scatterer location, this leads to a coherent field summation over the entire bandwidth, whereas at other locations the summation is only incoherent.

The effects of dispersion and conductive losses on TD-DORT performance have been considered using realistic soil types. It has been observed that, although losses result in degradation on the TRO eigenvalue magnitudes, scatterer localization can still be extracted from phase information. Using the existing phase information along with attenuation compensation results in a focusing performance closer to that achieved in the NDL case. For cases where background medium is *both* inhomogeneous and lossy, and only statistical information is available on the intervening medium, it is not possible to exactly compensate for losses. However, partial compensation can be achieved for low fluctuations and losses by employing time-dependent inverse filters constructed using ensemble averages.

Only impenetrable, well-resolved point-like scatterers have been considered here. Parameters such as number of antennas, spacing, and frequency of operation also play an important role in the overall performance. Depending on the particular application in mind, these parameters can be optimized to further improve selective focusing capabilities of UWB DORT in inhomogeneous, random media.

## REFERENCES

[1] M. Fink, D. Cassereau, A. Derode, C. Prada, P. Roux, M. Tanter, J. Thomas, and F. Wu, "Time-reversed acoustics," *Rep. Prog. Phys.*, vol. 63, pp. 1933–1995, 2000.

[2] J. L. Thomas, F. Wu, and M. Fink, "Time reversal focusing applied to lithotripsy," *Ultrason. Imag.*, vol. 18, no. 2, pp. 106–121, Apr. 1996.

[3] J. L. Thomas, P. Roux, and M. Fink, "Inverse scattering analysis with an acoustic time-reversal mirror," *Phys. Rev. Lett.*, vol. 72, no. 5, pp. 637–640, Jan. 1994.

[4] G. F. Edelmann, T. Akal, W. S. Hodgkiss, S. Kim, W. A. Kuperman, and H. C. Song, "An initial demonstration of underwater acoustic communications using time reversal," *IEEE J. Oceanic Eng.*, vol. 27, pp. 602–609, Jul. 2002.

[5] P. Kyritsi, G. Papanicolaou, P. Eggers, and A. Oprea, "MISO time reversal and delay-spread compression for FWA channels at 5 GHz," *IEEE Antennas and Wireless Prop. Lett.*, vol. 3, pp. 96–99, 2004.

[6] B. E. Henty and D. D. Stancil, "Multipath-enabled super-resolution for rf and microwave communication using phase-conjugate arrays," *Phys. Rev. Lett.*, vol. 93, no. 24, pp. 243 904/1–243 904/4, 2004.

[7] M. E. Yavuz and F. L. Teixeira, "A numerical study of time reversed UWB electromagnetic waves in continuous random media," *IEEE Antennas Wireless Prop. Lett.*, vol. 4, pp. 43–46, 2005.

[8] P. Kosmas and C. M. Rappaport, "Time reversal with the fdtd method for microwave breast cancer detection," *IEEE Trans. Microwave Theory Tech.*, vol. 53, pp. 2317–2323, Jul. 2005.

[9] F. K. Gruber, E. A. Marengo, and A. J. Devaney, "Time-reversal imaging with multiple signal classification considering multiple scattering between the targets," *J. Acoust. Soc. Amer.*, vol. 115, pp. 3042–3047, 2004.

[10] A. J. Devaney, "Time reversal imaging of obscured targets from multistatic data," *IEEE Trans. Antennas Propag.*, vol. 53, no. 5, pp. 1600–1610, May 2005.

[11] A. J. Devaney, E. A. Marengo, and F. K. Gruber, "Time-reversal-based imaging and inverse scattering of multiply scattering point targets," *J. Acoust. Soc. Amer.*, vol. 118, pp. 3129–3138, 2005.

[12] D. H. Liu, G. Kang, L. Li, Y. Chen, S. Vasudevan, W. Joines, Q. H. Liu, J. Krolik, and L. Carin, "Electromagnetic time-reversal imaging of a target in a cluttered environment," *IEEE Trans. Antennas Propag.*, vol. 53, pp. 3058–3066, Sep. 2005.

[13] D. H. Chambers and J. G. Berryman, "Analysis of the time-reversal operator for a small spherical scatterer in an electromagnetic field," *IEEE Trans. Antennas Propag.*, vol. 52, no. 7, pp. 1729–1738, Jul. 2004.

[14] H. Zhao, "Analysis of the response matrix for an extended target," *SIAM J. Appl. Math.*, vol. 64, no. 3, pp. 725–745, 2004.

[15] C. Prada and M. Fink, "Eigenmodes of the time reversal operator: a solution to selective focusing in multiple-target media," *Wave Motion*, vol. 20, pp. 151–163, 1994.

[16] C. Prada, S. Mannevile, D. Spoliansky, and M. Fink, "Decomposition of the time reversal operator: detection and selective focusing on two scatterers," *J. Acoust. Soc. Amer.*, vol. 99, pp. 2067–2076, 1996.

[17] H. Tortel, G. Micolau, and M. Saillard, "Decomposition of the time reversal operator for electromagnetic scattering," *J. Electromagn. Waves Appl.*, vol. 13, pp. 687–719, 1999.

[18] G. Micolau and M. Saillard, "DORT method as applied to electromagnetic sensing of buried objects," *Radio Sci.*, vol. 38, no. 3, pp. 4-1–4-12, 2003.

[19] M. Saillard, P. Vincent, and G. Micolau, "Reconstruction of buried objects surrounded by small inhomogeneities," *Inverse Prob.*, vol. 16, no. 5, pp. 1195–1208, Oct. 2000.

[20] G. Micolau, M. Saillard, and P. Borderies, "DORT method as applied to ultrawideband signals for detection of buried objects," *IEEE Trans. Geosci. Remote Sensing*, vol. 41, no. 8, pp. 1813–1820, Aug. 2003.

[21] M. Tanter, J. L. Thomas, and M. Fink, "Focusing and steering through absorbing and aberrating layers: application to ultrasonic propagation through the skull," *J. Acoust. Soc. Amer.*, vol. 103, pp. 2403–2410, May 1998.

[22] T. Folégot, C. Prada, and M. Fink, "Resolution enhancement and separation of reverbaration from target echo with the time reversal operator decomposition," *J. Acoust. Soc. Amer.*, vol. 113, pp. 3155–3160, Jun. 2003.

[23] M. E. Yavuz and F. L. Teixeira, "Frequency dispersion compensation in time reversal techniques for UWB electromagnetic waves," *IEEE Geosci. Remote Sensing Lett.*, vol. 2, no. 2, pp. 233–237, Apr. 2005.

[24] C. Prada, J.-L. Thomas, and M. Fink, "The iterative time reversal process: analysis of the convergence," *J. Acoust. Soc. Amer.*, vol. 97, pp. 62–71, 1995.

[25] C. Tsogka and G. Papanicolaou, "Time reversal through a solid-liquid interface and super-resolution," *Inverse Prob.*, vol. 18, no. 6, pp. 1639–1657, 2002.

[26] A. Taflove, *Computational Electrodynamics: The Finite-Difference Time-Domain Method*. Norwood, MA: Artech House, 1995.

[27] C. D. Moss, F. L. Teixeira, Y. E. Yang, and J. A. Kong, "Finite-difference time-domain simulation of scattering from objects in continuous random media," *IEEE Trans. Geosci. Remote Sensing*, vol. 40, pp. 178–186, Jan. 2002.

[28] F. L. Teixeira, W. C. Chew, M. Straka, M. L. Oristaglio, and T. Wang, "Finite-difference time-domain simulation of ground penetrating radar on dispersive, inhomogeneous and conductive soils," *IEEE Trans. Geosci. Remote Sensing*, vol. 36, pp. 1928–1937, Nov. 1998.

[29] J. P. Berenger, "A perfectly matched layer for the absorption of electromagnetic waves," *J. Comput. Phys.*, vol. 114, pp. 185–200, 1994.

[30] F. J. Harris, "On the use of windows for harmonic analysis with the discrete Fourier transform," *Proc. IEEE*, vol. 66, pp. 51–83, Jan. 1978.

[31] J. E. Hipp, "Soil electromagnetic parameters as functions of frequency, soil density and soil moisture," *Proc. IEEE*, vol. 62, pp. 98–103, 1974.

[32] F. L. Teixeira and W. C. Chew, "On causality and dynamic stability of perfectly matched layers for fdtd simulations," *IEEE Trans. Microwave Theory Tech.*, vol. 47, pp. 775–785, Jun. 1999.

[33] G. Papanicolaou, L. Ryzhik, and K. Solna, "Statistical stability in time reversal," *SIAM J. Appl. Math.*, vol. 64, no. 4, pp. 1133–1155, 2004.

[34] A. Derode, A. Tourin, J. de Rosny, M. Tanter, S. Yon, and M. Fink, "Taking advantage of multiple scattering to communicate with time-reversal antennas," *Phys. Rev. Lett.*, vol. 90, no. 1, pp. 014301/1–014301/4, 2003.

[35] C. Rappaport, "A color map for effective black-and-white rendering of color-scale images," *IEEE Antennas Propag. Mag.*, vol. 44, no. 3, pp. 94–96, Jun. 2002.

[36] H. Lev-Ari and A. J. Devaney, "The time reversal techniques re-interpreted: subspace-based signal processing for multistatic target location," in *Proc. IEEE Sensor Array and Multichannel Signal Processing Workshop*, Mar. 2000, pp. 509–513.

[37] W. C. Chew, *Waves and Fields in Inhomogeneous Media*. New York: Van Nostrand Reinhold, 1990, reprinted by IEEE Press, 1995.

**Mehmet E. Yavuz** (S'00) was born in Erzurum, Turkey. He received the B.S. degree from the Middle East Technical University (METU), Ankara, Turkey, in 2001 and the M.S. degree from the Koc University, Istanbul, Turkey, in 2003, both in electrical engineering. He is currently working toward the Ph.D. degree in electrical engineering at the ElectroScience Laboratory of The Ohio State University, Columbus.

His current research interests include time-reversal methods for electromagnetics, microwave imaging and detection, inverse scattering and computational electromagnetics.

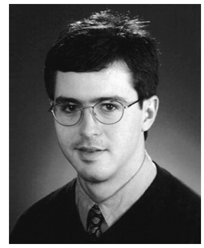

**Fernando L. Teixeira** (S'89–M'93–SM'05) received the B.S. and M.S. degrees in electrical engineering from the Pontifical Catholic University of Rio de Janeiro (PUC-Rio), Brazil, in 1991 and 1995, respectively, and the Ph.D. degree in electrical engineering from the University of Illinois at Urbana-Champaign, in 1999.

From 1999 to 2000, he was a Postdoctoral Research Associate with the Research Laboratory of Electronics, Massachusetts Institute of Technology (MIT), Cambridge. Since 2000, he has been an Assistant Professor in the ElectroScience Laboratory and the Department of Electrical and Computer Engineering, The Ohio State University, Columbus. His current research interests include analytical and numerical techniques for wave propagation and scattering problems in communication, sensing, and devices applications. He has edited one book *Geometric Methods for Computational Electromagnetics* (Cambridge, MA: PIER 32 EMW, 2001), coauthored more than 60 journal articles and book chapters, and more than 90 conference papers in those areas.

Dr. Teixeira is a Member of Phi Kappa Phi, Sigma Xi, and a Full Member of the International Scientific Radio Union (URSI) Commission B. He was awarded many prizes for his research including the NSF CAREER Award in 2004 and the triennial USNC/URSI Booker Fellowship in 2005.